OpenSTL: A Comprehensive Benchmark of Spatio-Temporal Predictive Learning

Cheng Tan[1,2*] **Siyuan Li**[1,2*] **Zhangyang Gao**[1,2] **Wenfei Guan**[3] **Zedong Wang**[2]
Zicheng Liu[1,2] **Lirong Wu**[1,2] **Stan Z. Li**[2†]
[1]Zhejiang University; [3]Xidian University;
[2]AI Lab, Research Center for Industries of the Future, Westlake University
{tancheng; lisiyuan; gaozhangyang; guanwenfei; wangzedong; liuzicheng;
wulirong; stan.zq.li}@westlake.edu.cn;

Abstract

Spatio-temporal predictive learning is a learning paradigm that enables models to learn spatial and temporal patterns by predicting future frames from given past frames in an unsupervised manner. Despite remarkable progress in recent years, a lack of systematic understanding persists due to the diverse settings, complex implementation, and difficult reproducibility. Without standardization, comparisons can be unfair and insights inconclusive. To address this dilemma, we propose OpenSTL, a comprehensive benchmark for spatio-temporal predictive learning that categorizes prevalent approaches into recurrent-based and recurrent-free models. OpenSTL provides a modular and extensible framework implementing various state-of-the-art methods. We conduct standard evaluations on datasets across various domains, including synthetic moving object trajectory, human motion, driving scenes, traffic flow, and weather forecasting. Based on our observations, we provide a detailed analysis of how model architecture and dataset properties affect spatio-temporal predictive learning performance. Surprisingly, we find that recurrent-free models achieve a good balance between efficiency and performance than recurrent models. Thus, we further extend the common MetaFormers to boost recurrent-free spatial-temporal predictive learning. We open-source the code and models at https://github.com/chengtan9907/OpenSTL.

1 Introduction

Recent years have witnessed rapid and remarkable progress in spatio-temporal predictive learning [38, 29, 10, 41]. This burgeoning field aims to learn latent spatial and temporal patterns through the challenging task of forecasting future frames based solely on given past frames in an unsupervised manner [40, 55, 56, 54]. By ingesting raw sequential data, these self-supervised models [4, 14, 24] can uncover intricate spatial and temporal interdependencies without the need for tedious manual annotation, enabling them to extrapolate coherently into the future in a realistic fashion [29, 12]. Spatio-temporal predictive learning benefits a wide range of applications with its ability to anticipate the future from the past in a data-driven way, including modeling the devastating impacts of climate change [38, 35], predicting human movement [61, 45], forecasting traffic flow in transportation systems [8, 51], and learning expressive representations from video [32, 19]. By learning to predict the future without supervision from massive datasets, these techniques have the potential to transform domains where anticipation and planning are crucial but limited labeled data exists [9, 2, 44, 31].

[*] Equal contribution.
[†] Corresponding author.

37th Conference on Neural Information Processing Systems (NeurIPS 2023) Track on Datasets and Benchmarks.

https://doi.org/10.52202/075280-3060

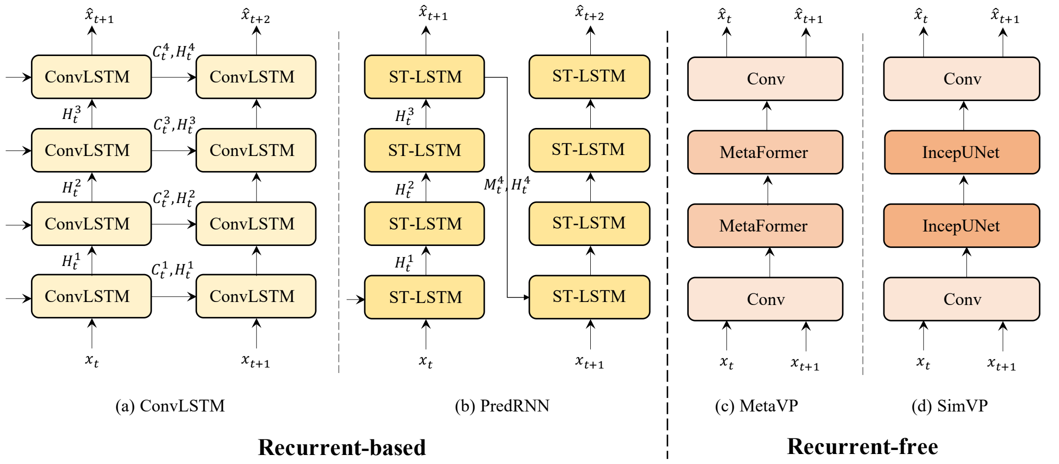

(a) ConvLSTM (b) PredRNN (c) MetaVP (d) SimVP

Figure 1: Two typical sptaio-temporal predictive learning models. As illustrated by the left two instances (a)(b), the first type requires several recurrent modules to predict the next frame according to the previous frames in an auto-regressive manner, dubbed recurrent-based models. As for the right two instances (c)(d), the second type predicts all future frames based on all given frames at once, which inferences in parallel and is called the recurrent-free model.

Despite the significance of spatio-temporal predictive learning and the development of various approaches, there remains a conspicuous lack of a comprehensive benchmark for this field covering various synthetic and practical application scenarios. We believe that a comprehensive benchmark is essential for advancing the field and facilitating meaningful comparisons between different methods. In particular, there exists a perennial question that has not yet been conclusively answered: *is it necessary to employ recurrent neural network architectures to capture temporal dependencies?* In other words, *can recurrent-free models achieve performance comparable to recurrent-based models without explicit temporal modeling*?

Since the seminal work ConvLSTM [38] was proposed, which ingeniously integrates convolutional networks and long-short term memory (LSTM) networks [15] to separately capture spatial and temporal correlations, researchers have vacillated between utilizing or eschewing recurrent architectures. As shown in Figure 1, (a) ConvLSTM is a prototypical recurrent-based model that infuses a recurrent structure into convolutional networks. (b) PredRNN [49] represents a series of recurrent models that revise the flow of information to enhance performance. (c) MetaVP is the recurrent-free model that abstracted from SimVP by substituting its IncepU [10] modules with MetaFormers [59]. (d) SimVP [10, 40] is a typical recurrent-free model that achieves performance comparable to previous state-of-the-art models without explicitly modeling temporal dependencies.

In this study, we illuminate the long-standing question of whether explicit temporal modeling with recurrent neural networks is requisite for spatio-temporal predictive learning. To achieve this, we present a comprehensive benchmark, **Open S**patio-**T**emporal predictive **L**earning, dubbed OpenSTL. We revisit the approaches that represent the foremost strands within a modular and extensive framework to ensure fair comparisons. We summarize our main contributions as follows:

- We build OpenSTL, a comprehensive benchmark for spatio-temporal predictive learning that includes 14 representative algorithms and 24 models. OpenSTL covers a wide range of methods and classifies them into two categories: recurrent-based and recurrent-free methods.
- We conduct extensive experiments on a diversity of tasks ranging from synthetic moving object trajectories to real-world human motion, driving scenes, traffic flow, and weather forecasting. The datasets span synthetic to real-world data and micro-to-macro scales.
- While recurrent-based models have been well developed, we rethink the potential of recurrent-free models based on insights from OpenSTL. We propose generalizing MetaFormer-like architectures [59] to boost recurrent-free spatio-temporal predictive learning. Recurrent-free models can thus reformulate the problem as a downstream task of designing vision backbones for general applications.

https://doi.org/10.52202/075280-3060

2 Background and Related work

2.1 Problem definition

We propose the formal definition for the spatio-temporal predictive learning problem as follows. Given a sequence of video frames $\mathcal{X}^{t,T} = \{\boldsymbol{x}^i\}_{t-T+1}^{t}$ up to time t spanning the past T frames, the objective is to predict the subsequent T' frames $\mathcal{Y}^{t+1,T'} = \{\boldsymbol{x}^i\}_{t+1}^{t+1+T'}$ from time $t+1$ onwards, where each frame $\boldsymbol{x}_i \in \mathbb{R}^{C \times H \times W}$ typically comprises C channels, with height H and width W pixels. In practice, we represent the input sequence of observed frames and output sequence of predicted frames respectively as tensors $\mathcal{X}^{t,T} \in \mathbb{R}^{T \times C \times H \times W}$ and $\mathcal{Y}^{t+1,T'} \in \mathbb{R}^{T' \times C \times H \times W}$.

The model with learnable parameters Θ learns a mapping $\mathcal{F}_\Theta : \mathcal{X}^{t,T} \mapsto \mathcal{Y}^{t+1,T'}$ by leveraging both spatial and temporal dependencies. In our case, the mapping $\mathcal{F}_\Theta$ corresponds to a neural network trained to minimize the discrepancy between the predicted future frames and the ground-truth future frames. The optimal parameters Θ^* are given by:

$$\Theta^* = \arg\min_{\Theta} \mathcal{L}(\mathcal{F}_\Theta(\mathcal{X}^{t,T}), \mathcal{Y}^{t+1,T'}), \tag{1}$$

where $\mathcal{L}$ denotes a loss function that quantifies such discrepancy.

In this study, we categorize prevalent spatio-temporal predictive learning methods into two classes: recurrent-based and recurrent-free models. For *recurrent-based models*, the mapping $\mathcal{F}_\Theta$ comprises several recurrent interactions:

$$\mathcal{F}_\Theta : f_\theta(\boldsymbol{x}^{t-T+1}, \boldsymbol{h}^{t-T+1}) \circ ... \circ f_\theta(\boldsymbol{x}^{t}, \boldsymbol{h}^{t}) \circ ... \circ f_\theta(\boldsymbol{x}^{t+T'-1}, \boldsymbol{h}^{t+T'-1}), \tag{2}$$

where $\boldsymbol{h}^i$ represents the memory state encompassing historical information and f_θ denotes the mapping between each pair of adjacent frames. The parameters θ are shared across each state. Therefore, the prediction process can be expressed as follows:

$$\boldsymbol{x}^{t+1} = f_\theta(\boldsymbol{x}^i, \boldsymbol{h}^i), \forall i \in \{t+1, \cdots, t+T'\}, \tag{3}$$

For *recurrent-free* models, the prediction process directly feeds the whole sequence of observed frames into the model and outputs the complete predicted frames at once.

2.2 Recurrent-based models

Since the pioneering work ConvLSTM [38] was proposed, recurrent-based models [29, 30, 16, 12, 58, 31] have been extensively studied. PredRNN [49] adopts vanilla ConvLSTM modules to build a Spatio-temporal LSTM (ST-LSTM) unit that models spatial and temporal variations simultaneously. PredRNN++ [47] proposes a gradient highway unit to mitigate the gradient vanishing and a Casual-LSTM module to cascadely connect spatial and temporal memories. PredRNNv2 [50] further proposes a curriculum learning strategy and a memory decoupling loss to boost performance. MIM [51] introduces high-order non-stationarity learning in designing LSTM modules. PhyDNet [12] explicitly disentangles PDE dynamics from unknown complementary information with a recurrent physical unit. E3DLSTM [48] integrates 3D convolutions into recurrent networks. MAU [3] proposes a motion-aware unit that captures motion information. Although various recurrent-based models have been developed, the reasons behind their strong performance remain not fully understood.

2.3 Recurrent-free models

Compared to recurrent-based models, recurrent-free models have received less attention. Previous studies tend to use 3D convolutional networks to model temporal dependencies [28, 1]. PredCNN [57] and TrajectoryCNN [25] use 2D convolutional networks for efficiency. However, early recurrent-free models were doubted due to their poor performance. Recently, SimVP [10, 40, 41] provided a simple but effective recurrent-free baseline with competitive performance. PastNet [53] and IAM4VP [37] are two recent recurrent-free models that perform strong performance. In this study, we implemented representative recurrent-based and recurrent-free models under a unified framework to systematically investigate their intrinsic properties. Moreover, we further explored the potential of recurrent-free models by reformulating the spatio-temporal predictive learning problem and extending MetaFormers [59] to bridge the gap between the visual backbone and spatio-temporal learning.

https://doi.org/10.52202/075280-3060

3 OpenSTL

3.1 Supported Methods

3.1.1 Overview

OpenSTL has implemented 14 representative spatio-temporal predictive learning methods under a unified framework, including 11 recurrent-based methods and 3 recurrent-free methods. We summarize these methods in Table 1, where we also provide the corresponding conference/journal and the types of their spatial-temporal modeling components. The spatial modeling of these methods is fundamentally consistent. Most methods apply two-dimensional convolutional networks (Conv2D) to model spatial dependencies, while E3D-LSTM and CrevNet harness three-dimensional convolutional networks (Conv3D) instead.

The primary distinction between these methods lies in how they model temporal dependencies using their proposed modules. The ST-LSTM module, proposed in PredRNN [49], is the most widely used module. CrevNet has a similar modeling approach as PredRNN, but it incorporates an information-preserving mechanism into the model. Analogously, Casual-LSTM [47], MIM Block [51], E3D-LSTM [48], PhyCell [12], and MAU [3] represent variants of ConvLSTM proposed with miscellaneous motivations. MVFB is built as a multi-scale voxel flow block that diverges from ConvLSTM. However, DMVFN [17] predicts future frames frame-by-frame which still qualifies as a recurrent-based model. IncepU [10] constitutes an Unet-like module that also exploits the multi-scale feature from the InceptionNet-like architecture. gSTA [40] and TAU [41] extend the IncepU module to simpler and more efficient architectures without InceptionNet or Unet-like architectures. In this work, we further extend the temporal modeling of recurrent-free models by introducing MetaFormers [59] to boost recurrent-free spatio-temporal predictive learning.

Table 1: Categorizations of the supported spatial-temporal predictive learning methods in OpenSTL.

Category	Method	Conference/Journal	Spatial modeling	Temporal modeling
Recurrent-based	ConvLSTM [38]	NeurIPS 2015	Conv2D	Conv-LSTM
	PredNet [29]	ICLR 2017	Conv2D	ST-LSTM
	PredRNN [49]	NeurIPS 2017	Conv2D	ST-LSTM
	PredRNN++ [47]	ICML 2018	Conv2D	Casual-LSTM
	MIM [51]	CVPR 2019	Conv2D	MIM Block
	E3D-LSTM [48]	ICLR 2019	Conv3D	E3D-LSTM
	CrevNet [58]	ICLR 2020	Conv3D	ST-LSTM
	PhyDNet [12]	CVPR 2020	Conv2D	ConvLSTM+PhyCell
	MAU [3]	NeurIPS 2021	Conv2D	MAU
	PredRNNv2 [50]	TPAMI 2022	Conv2D	ST-LSTM
	DMVFN [17]	CVPR 2023	Conv2D	MVFB
Recurrent-free	SimVP [10]	CVPR 2022	Conv2D	IncepU
	TAU [41]	CVPR 2023	Conv2D	TAU
	SimVPv2 [40]	arXiv	Conv2D	gSTA

3.1.2 Rethink the recurrent-free models

Although less studied, recurrent-free spatio-temporal predictive learning models share a similar architecture, as illustrated in Figure 2. The encoder comprises several 2D convolutional networks, which project high-dimensional input data into a low-dimensional latent space. When given a batch of input observed frames $\mathcal{B} \in \mathbb{R}^{B\times T\times C\times H\times W}$, the encoder focuses solely on intra-frame spatial correlations, ignoring temporal modeling. Subsequently, the middle temporal module stacks the low-dimensional representations along the temporal dimension to ascertain temporal dependencies. Finally, the decoder comprises several 2D convolutional upsampling networks, which reconstruct subsequent frames from the learned latent representations.

The encoder and decoder enable efficient temporal learning by modeling temporal dependencies in a low-dimensional latent space. The core component of recurrent-free models is the temporal module. Previous studies have proposed temporal modules such as IncepU [10], TAU [41], and

https://doi.org/10.52202/075280-3060

gSTA [40] that have proved beneficial. However, we argue that the competence stems primarily from the general recurrent-free architecture instead of the specific temporal modules. Thus, we employ MetaFormers [59] as the temporal module by changing the input channels from the original C to inter-frame channels $T \times C$. By extending the recurrent-free architecture, we leverage the advantages of MetaFormers to enhance the recurrent-free model. In this work, we implement ViT [7], Swin Transformer [26], Uniformer [21], MLP-Mixer [42], ConvMixer [43], Poolformer [59], ConvNeXt [27], VAN [13], HorNet [33], and MogaNet [22] for the MetaFormers-based recurrent-free model, substituting the intermediate temporal module in the original recurrent-free architecture.

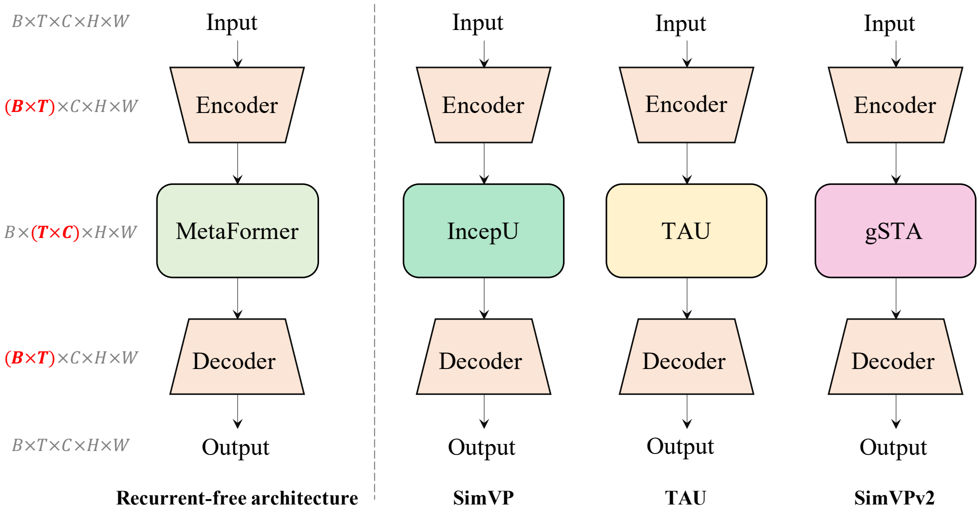

Figure 2: The general architecture of recurrent-free models with three instances.

3.2 Supported Tasks

We have curated five diverse tasks in our OpenSTL benchmark, which cover a wide range of scenarios from synthetic simulations to real-world situations at various scales. The tasks include synthetic moving object trajectories, real-world human motion capture, driving scenes, traffic flow, and weather forecasting. The datasets used in our benchmark range from synthetic to real-world, and from micro to macro scales. We have provided a summary of the dataset statistics in Table 2.

Table 2: The detailed dataset statistics of the supported tasks in OpenSTL.

Dataset	Training size	Testing size	Channel	Height	Width	T	T'
Moving MNIST variants	10,000	10,000	1 / 3	64	64	10	10
KTH Action	4,940	3,030	1	128	128	10	20/40
Human3.6M	73,404	8,582	3	128	128	4	4
Kitti&Caltech	3,160	3,095	3	128	160	10	1
TaxiBJ	20,461	500	2	32	32	4	4
WeatherBench-S	2,167	706	1	32/128	64/256	12	12
WeatherBench-M	54,019	2,883	4	32	64	4	4

Synthetic moving object trajectory prediction *Moving MNIST* [39] is one of the seminal benchmark datasets that has been extensively utilized. Each video sequence comprises two moving digits confined within a 64×64 frame. Each digit was assigned a velocity whose direction was randomly chosen from a unit circle and whose magnitude was also arbitrarily selected from a fixed range. Apart from the original Moving MNIST dataset, we provide two variants with more complicated objects (*Moving FashionMNIST*) that replace the digits with fashion objects and more complex scenes (*Moving MNIST-CIFAR*) that employ images from the CIFAR-10 dataset [20] as the background. Moreover, we provide three settings of Moving MNIST for robustness evaluations, including missing frames, dynamic noise, and perceptual occlusions.

Human motion capture Predicting human motion is challenging due to the complexity of human movements, which vary greatly among individuals and actions. We utilized the *KTH* dataset [36], which includes six types of human actions: walking, jogging, running, boxing, hand waving, and hand clapping. We furnish two settings, predicting the next 20 and 40 frames respectively. *Human3.6M* [18] is an intricate human pose dataset containing high-resolution RGB videos. Analogous to preceding studies [12, 51], we predict the next four frames by the observed four frames.

Driving scene prediction Predicting the future dynamics of driving scenarios is crucial for autonomous driving. Compared to other tasks, this undertaking involves non-stationary and diverse scenes. To address this issue, we follow the conventional approach [29] and train the model on the *Kitti* [11] dataset. We then evaluate the performance on the *Caltech Pedestrian* [6] dataset. To ensure consistency, we center-cropped and downsized all frames to 128 × 160 pixels.

Traffic flow prediction Forecasting the dynamics of crowds is crucial for traffic management and public safety. To evaluate spatio-temporal predictive learning approaches for traffic flow prediction, we use the *TaxiBJ* [60] dataset. This dataset includes GPS data from taxis and meteorological data in Beijing. The dataset contains two types of crowd flows, representing inflow and outflow. The temporal interval is 30 minutes, and the spatial resolution is 32 × 32.

Weather forecasting Global weather pattern prediction is an essential natural predicament. The WeatherBench [34] dataset is a large-scale weather forecasting dataset encompassing various types of climatic factors. The raw data is re-grid to 5.625° resolution (32 × 64 grid points) and 1.40625° (128 × 256 grid points). We consider two setups: First, *WeatherBench-S* is a single-variable setup in which each climatic factor is trained independently. The model is trained on data from 2010-2015, validated on data from 2016, and tested on data from 2017-2018, with a one-hour temporal interval. Second, *WeatherBench-M* is a multi-variable setup that mimics real-world weather forecasting more closely. All climatic factors are trained simultaneously. The model is trained on data from 1979 to 2015, using the same validation and testing data as WeatherBench-S. The temporal interval is extended to six hours, capturing a broader range of temporal dependencies.

3.3 Evaluation Metrics

We evaluate the performance of supported models on the aforementioned tasks using various metrics in a thorough and rigorous manner. We use them for specific tasks according to their characteristics.

Error metrics We utilize the mean squared error (MSE) and mean absolute error (MAE) to evaluate the difference between the predicted results and the true targets. Root mean squared error (RMSE) is also used in weather forecasting as it is more common in this domain.

Similarity metrics We utilize the structural similarity index measure (SSIM) [52] and peak signal-to-noise ratio (PSNR) to evaluate the similarity between the predicted results and the true targets. Such metrics are extensively used in image processing and computer vision.

Perceptual metrics LPIPS [62] is implemented to evaluate the perceptual difference between the predicted results and the true targets in the human visual system. LPIPS provides a perceptually-aligned evaluation for vision tasks. We utilize this metric in real-world video prediction tasks.

Computational metrics We utilize the number of parameters and the number of floating-point operations (FLOPs) to evaluate the computational complexity of the models. We also report the frames per second (FPS) on a single NVIDIA V100 GPU to evaluate the inference speed.

3.4 Codebase Structure

While existing open-sourced spatio-temporal predictive learning codebases are independent, OpenSTL provides a modular and extensible framework that adheres to the design principles of OpenMMLab [5] and assimilates code elements from OpenMixup [23] and USB [46]. OpenSTL excels in user-friendliness, organization, and comprehensiveness, surpassing the usability of existing open-source STL codebases. A detailed description of the codebase structure can be found in Appendix B.

https://doi.org/10.52202/075280-3060

4 Experiment and Analysis

We conducted comprehensive experiments on the mentioned tasks to assess the performance of the supported methods in OpenSTL. Detailed analysis of the results is presented to gain insights into spatio-temporal predictive learning. Implementation details can be found in Appendix C.

4.1 Synthetic Moving Object Trajectory Prediction

We conduct experiments on the synthetic moving object trajectory prediction task, utilizing three datasets: Moving MNIST, Moving FashionMNIST, and Moving MNIST-CIFAR. The performance of the evaluated models on the Moving MNIST dataset is reported in Table 3. The detailed results for the other two synthetic datasets are in Appendix D.1.

It can be observed that recurrent-based models yield varied results that do not consistently outperform recurrent-free models, while recurrent-based models always exhibit slower inference speeds than their recurrent-free counterparts. Although PredRNN, PredRNN++, MIM, and PredRNNv2 achieve lower MSE and MAE values compared to recurrent-free models, their FLOPs are nearly five times higher, and their FPS are approximately seven times slower than all recurrent-free models. Furthermore, there are minimal disparities in the performance of recurrent-free models as opposed to recurrent-based models, highlighting the robustness of the proposed general recurrent-free architecture. The remaining two synthetic datasets, consisting of more intricate moving objects (Moving FashionMNIST) and complex scenes (Moving MNIST-CIFAR), reinforce the experimental findings that recurrent-free models deliver comparable performance with significantly higher efficiency. In these toy datasets characterized by high frequency but low resolution, recurrent-based models excel in capturing temporal dependencies but are susceptible to high computational complexity.

Table 3: The performance on the Moving MNIST dataset.

Method		Params (M)	FLOPs (G)	FPS	MSE ↓	MAE ↓	SSIM ↑	PSNR ↑
Recurrent-based	ConvLSTM	15.0	56.8	113	29.80	90.64	0.9288	22.10
	PredNet	12.5	8.4	659	161.38	201.16	0.7783	14.67
	PredRNN	23.8	116.0	54	23.97	72.82	0.9462	23.28
	PredRNN++	38.6	171.7	38	**22.06**	**69.58**	**0.9509**	**23.65**
	MIM	38.0	179.2	37	22.55	69.97	0.9498	23.56
	E3D-LSTM	51.0	298.9	18	35.97	78.28	0.9320	21.11
	CrevNet	5.0	270.7	10	30.15	86.28	0.9350	22.15
	PhyDNet	3.1	15.3	182	28.19	78.64	0.9374	22.62
	MAU	4.5	17.8	201	26.86	78.22	0.9398	22.57
	PredRNNv2	23.9	116.6	52	24.13	73.73	0.9453	23.21
	DMVFN	3.5	0.2	1145	123.67	179.96	0.8140	16.15
Recurrent-free	SimVP	58.0	19.4	209	32.15	89.05	0.9268	21.84
	TAU	44.7	16.0	283	24.60	71.93	0.9454	23.19
	SimVPv2	46.8	16.5	282	26.69	77.19	0.9402	22.78
	ViT	46.1	16.9	290	35.15	95.87	0.9139	21.67
	Swin Transformer	46.1	16.4	294	29.70	84.05	0.9331	22.22
	Uniformer	44.8	16.5	296	30.38	85.87	0.9308	22.13
	MLP-Mixer	38.2	14.7	334	29.52	83.36	0.9338	22.22
	ConvMixer	3.9	5.5	658	32.09	88.93	0.9259	21.93
	Poolformer	37.1	14.1	341	31.79	88.48	0.9271	22.03
	ConvNext	37.3	14.1	344	26.94	77.23	0.9397	22.74
	VAN	44.5	16.0	288	26.10	76.11	0.9417	22.89
	HorNet	45.7	16.3	287	29.64	83.26	0.9331	22.26
	MogaNet	46.8	16.5	255	25.57	75.19	0.9429	22.99

4.2 Real-world Video Prediction

We perform experiments on real-world video predictions, specifically focusing on human motion capturing using the KTH and Human3.6M datasets, as well as driving scene prediction using the Kitti&Caltech dataset. Due to space constraints, we present the results for the Kitti&Caltech dataset in Table 4, while the detailed results for the other datasets can be found in Appendix D.2. We observed that as the resolution increases, the computational complexity of recurrent-based models dramatically increases. In contrast, recurrent-free models achieve a commendable balance between efficiency and performance. Notably, although some recurrent-based models achieve lower MSE and MAE values, their FLOPs are nearly 20 times higher compared to their recurrent-free counterparts. This highlights the efficiency advantage of recurrent-free models, especially in high-resolution scenarios.

Table 4: The performance on the Kitti&Caltech dataset.

Method		Params (M)	FLOPs (G)	FPS	MSE ↓	MAE ↓	SSIM ↑	PSNR ↑	LPIPS ↓
Recurrent-based	ConvLSTM	15.0	595.0	33	139.6	1583.3	0.9345	27.46	8.58
	PredNet	12.5	42.8	94	159.8	1568.9	0.9286	27.21	11.29
	PredRNN	23.7	1216.0	17	130.4	1525.5	0.9374	27.81	7.40
	PredRNN++	38.5	1803.0	12	**125.5**	**1453.2**	0.9433	28.02	13.21
	MIM	49.2	1858.0	39	125.1	1464.0	0.9409	**28.10**	6.35
	E3D-LSTM	54.9	1004.0	10	200.6	1946.2	0.9047	25.45	12.60
	PhyDNet	3.10	40.4	117	312.2	2754.8	0.8615	23.26	32.19
	MAU	24.3	172.0	16	177.8	1800.4	0.9176	26.14	9.67
	PredRNNv2	23.8	1223.0	16	147.8	1610.5	0.9330	27.12	8.92
	DMVFN	3.6	1.2	557	183.9	1531.1	0.9314	26.78	**4.94**
Recurrent-free	SimVP	8.6	60.6	57	160.2	1690.8	0.9338	26.81	6.76
	TAU	15.0	92.5	55	131.1	1507.8	0.9456	27.83	5.49
	SimVPv2	15.6	96.3	40	129.7	1507.7	0.9454	27.89	5.57
	ViT	12.7	155.0	25	146.4	1615.8	0.9379	27.43	6.66
	Swin Transformer	15.3	95.2	49	155.2	1588.9	0.9299	27.25	8.11
	Uniformer	11.8	104.0	28	135.9	1534.2	0.9393	27.66	6.87
	MLP-Mixer	22.2	83.5	60	207.9	1835.9	0.9133	26.29	7.75
	ConvMixer	1.5	23.1	129	174.7	1854.3	0.9232	26.23	7.76
	Poolformer	12.4	79.8	51	153.4	1613.5	0.9334	27.38	7.00
	ConvNext	12.5	80.2	54	146.8	1630.0	0.9336	27.19	6.99
	VAN	14.9	92.5	41	127.5	1476.5	0.9462	27.98	5.50
	HorNet	15.3	94.4	43	152.8	1637.9	0.9365	27.09	6.00
	MogaNet	15.6	96.2	36	131.4	1512.1	**0.9442**	27.79	5.39

4.3 Traffic and Weather Forecasting

Traffic flow prediction and weather forecasting are two critical tasks that have significant implications for public safety and scientific research. While these tasks operate at a macro level, they exhibit lower frequencies compared to the tasks mentioned above, and the states along the timeline tend to be more stable. Capturing subtle changes in such tasks poses a significant challenge. In order to assess the performance of the supported models in OpenSTL, we conduct experiments on the TaxiBJ and WeatherBench datasets. It is worth noting that weather forecasting encompasses various settings, and we provide detailed results of them in Appendix D.3.

Here, we present a comparison of the MAE and RMSE metrics for representative approaches in single-variable weather factor forecasting at low resolution. Figure 3 displays the results for four climatic factors, i.e., temperature, humidity, wind component, and cloud cover. Notably, recurrent-free models consistently outperform recurrent-based models across all weather factors, indicating their potential to apply spatio-temporal predictive learning to macro-scale tasks instead of relying solely on recurrent-based models. These findings underscore the promising nature of recurrent-free models and suggest that they can be a viable alternative to the prevailing recurrent-based models in

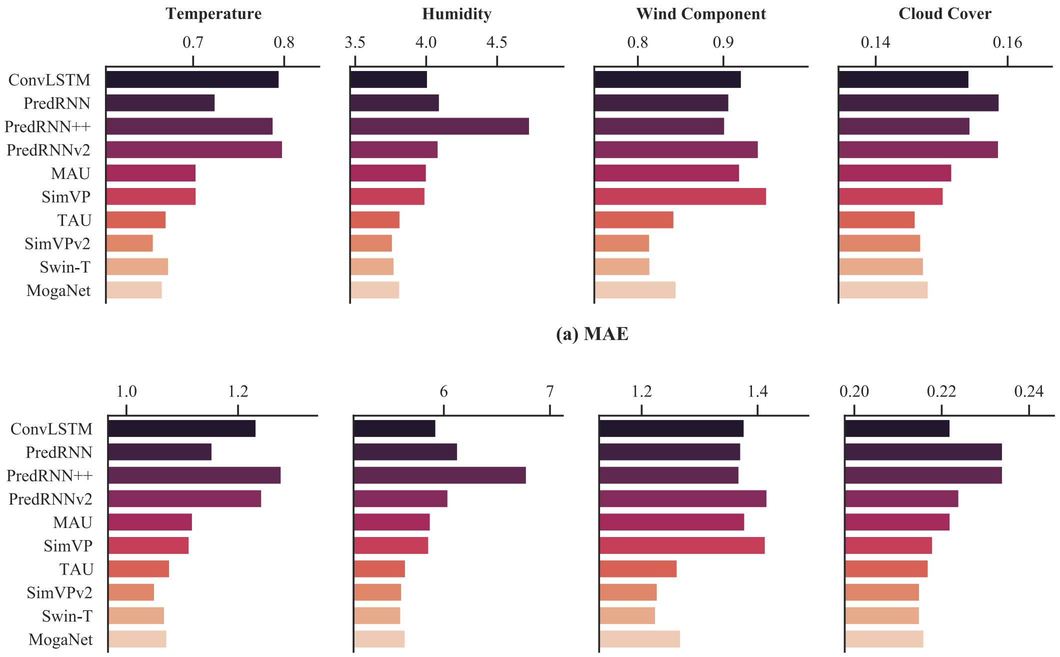

(a) MAE

(b) RMSE

Figure 3: The (a) MAE and (b) RMSE metrics of the representative approaches on the four weather forecasting tasks in WeatherBench.

the context of weather forecasting. Furthermore, in the Appendix, we provide additional insights into high-resolution and multi-variable weather forecasting, where similar trends are observed.

4.4 Robustness Analysis

To further understand the differences in robustness between the recurrent-based and recurrent-free spatiotemporal predictive learning methods, we constructed three experimental setups: (i) Moving MNIST - Missing, which deals with input frames with missing frames, where we set the probability of random missing frame to 20%; (ii) Moving MNIST - Dynamic, where we added random Gaussian noise to the speed of each digit, making their movement speeds irregular; (iii) Moving MNIST - Perceptual, where we randomly occluded the input frames, using a black 24×24 patch for occlusion. We choose three representative recurrent-based and three recurrent-free methods for evaluation. The experimental results for these three setups are presented in Table 5, 6, 7, respectively.

It can be observed that the recurrent-free methods exhibit remarkable robustness under both the missing and perceptual noise scenarios. Even when compared to situations without noise, there is little performance degradation due to their focus on global information. Conversely, recurrent-based methods encounter substantial performance drops. They overly focus on the relationships individual frames can inadvertently lead to overfitting. In the case of dynamic noise, all methods faced significant performance setbacks, because the speed of the digits became irregular and harder to predict.

Table 5: The performance on the Moving MNIST - Missing dataset.

Method		Params (M)	FLOPs (G)	FPS	MSE ↓	MAE ↓	SSIM ↑	PSNR ↑
Recurrent-based	ConvLSTM	15.0	56.8	113	32.73	96.95	0.9201	21.65
	PredRNN	23.8	116.0	54	46.05	117.21	0.8800	20.35
	PredRNN++	38.6	171.7	38	53.89	118.45	0.8907	19.71
Recurrent-free	SimVP	58.0	19.4	209	34.92	95.23	0.9194	21.44
	TAU	44.7	16.0	283	**26.77**	**77.50**	**0.9400**	**22.74**
	SimVPv2	46.8	16.5	282	28.63	81.79	0.9352	22.39

Table 6: The performance on the Moving MNIST - Dynamic dataset.

Method		Params (M)	FLOPs (G)	FPS	MSE ↓	MAE ↓	SSIM ↑	PSNR ↑
Recurrent-based	ConvLSTM	15.0	56.8	113	49.03	135.49	0.8683	19.73
	PredRNN	23.8	116.0	54	59.18	157.47	0.8220	19.09
	PredRNN++	38.6	171.7	38	**40.85**	**109.32**	**0.9030**	**20.65**
Recurrent-free	SimVP	58.0	19.4	209	48.41	130.83	0.8725	19.91
	TAU	44.7	16.0	283	43.37	121.31	0.8853	20.41
	SimVPv2	46.8	16.5	282	44.74	123.70	0.8823	20.28

Table 7: The performance on the Moving MNIST - Perceptual dataset.

Method		Params (M)	FLOPs (G)	FPS	MSE ↓	MAE ↓	SSIM ↑	PSNR ↑
Recurrent-based	ConvLSTM	15.0	56.8	113	31.34	95.39	0.9227	21.85
	PredRNN	23.8	116.0	54	46.04	122.40	0.8792	20.28
	PredRNN++	38.6	171.7	38	51.76	127.12	0.8722	19.85
Recurrent-free	SimVP	58.0	19.4	209	34.73	95.23	0.9196	21.44
	TAU	44.7	16.0	283	**26.87**	**78.08**	**0.9393**	**22.69**
	SimVPv2	46.8	16.5	282	28.83	82.65	0.9343	22.36

5 Conclusion and Discussion

This paper introduces OpenSTL, a comprehensive benchmark for spatio-temporal predictive learning with a diverse set of 14 representative methods and 24 models, addressing a wide range of challenging tasks. OpenSTL categorizes existing approaches into recurrent-based and recurrent-free models. To unlock the potential of recurrent-free models, we propose a general recurrent-free architecture and introduce MetaFormers for temporal modeling. Extensive experiments are conducted to systematically evaluate the performance of the supported models across various tasks. In synthetic datasets, recurrent-based models excel at capturing temporal dependencies, while recurrent-free models achieve comparable performance with significantly higher efficiency. In real-world video prediction tasks, recurrent-free models strike a commendable balance between efficiency and performance. Additionally, recurrent-free models demonstrate significant superiority over their counterparts in weather forecasting, highlighting their potential for scientific applications at a macro-scale level.

Moreover, we observed that *recurrent architectures are beneficial in capturing temporal dependencies, but they are not always necessary, especially for computationally expensive tasks*. Recurrent-free models can be a viable alternative that provides a good balance between efficiency and performance. The effectiveness of recurrent-based models in capturing high-frequency spatio-temporal dependencies can be attributed to their sequential tracking of frame-by-frame changes, providing a local temporal inductive bias. On the other hand, recurrent-free models combine multiple frames together, exhibiting a global temporal inductive bias that is suitable for low-frequency spatio-temporal dependencies. We hope that our work provides valuable insights and serves as a reference for future research.

While our primary focus lies in general spatio-temporal predictive learning, there are still several open problems that require further investigation. One particular challenge is finding ways to effectively leverage the strengths of both recurrent-based and recurrent-free models to enhance the modeling of spatial-temporal dependencies. While there is a correspondence between the spatial encoding and temporal modeling in MetaVP and the token mixing and channel mixing in MetaFormer, it raises the question of whether we can improve recurrent-free models by extending the existing MetaFormers.

Acknowledgments and Disclosure of Funding

This work was supported by the National Key R&D Program of China (2022ZD0115100), the National Natural Science Foundation of China (U21A20427), the Competitive Research Fund (WU2022A009) from the Westlake Center for Synthetic Biology and Integrated Bioengineering.

References

[1] S. Aigner and M. Körner. Futuregan: Anticipating the future frames of video sequences using spatio-temporal 3d convolutions in progressively growing gans. *arXiv preprint arXiv:1810.01325*, 2018.

[2] L. Castrejon, N. Ballas, and A. Courville. Improved conditional vrnns for video prediction. In *Proceedings of the IEEE/CVF International Conference on Computer Vision*, pages 7608–7617, 2019.

[3] Z. Chang, X. Zhang, S. Wang, S. Ma, Y. Ye, X. Xinguang, and W. Gao. Mau: A motion-aware unit for video prediction and beyond. *Advances in Neural Information Processing Systems*, 34, 2021.

[4] T. Chen, S. Kornblith, M. Norouzi, and G. Hinton. A simple framework for contrastive learning of visual representations. In *Proceedings of the International Conference on Machine Learning*, 2020.

[5] M. Contributors. MMCV: OpenMMLab computer vision foundation. https://github.com/open-mmlab/mmcv, 2018.

[6] P. Dollár, C. Wojek, B. Schiele, and P. Perona. Pedestrian detection: A benchmark. In *CVPR*, June 2009.

[7] A. Dosovitskiy, L. Beyer, A. Kolesnikov, D. Weissenborn, X. Zhai, T. Unterthiner, M. Dehghani, M. Minderer, G. Heigold, S. Gelly, et al. An image is worth 16x16 words: Transformers for image recognition at scale. In *International Conference on Learning Representations*.

[8] S. Fang, Q. Zhang, G. Meng, S. Xiang, and C. Pan. Gstnet: Global spatial-temporal network for traffic flow prediction. In *IJCAI*, pages 2286–2293, 2019.

[9] C. Finn, I. Goodfellow, and S. Levine. Unsupervised learning for physical interaction through video prediction. *Advances in Neural Information Processing Systems*, 29, 2016.

[10] Z. Gao, C. Tan, and S. Z. Li. Simvp: Simpler yet better video prediction. In *Proceedings of the IEEE/CVF Conference on Computer Vision and Pattern Recognition*, pages 3170–3180, 2022.

[11] A. Geiger, P. Lenz, C. Stiller, and R. Urtasun. Vision meets robotics: The kitti dataset. *The International Journal of Robotics Research*, 32(11):1231–1237, 2013.

[12] V. L. Guen and N. Thome. Disentangling physical dynamics from unknown factors for unsupervised video prediction. In *Proceedings of the IEEE/CVF Conference on Computer Vision and Pattern Recognition*, pages 11474–11484, 2020.

[13] M.-H. Guo, C.-Z. Lu, Z.-N. Liu, M.-M. Cheng, and S.-M. Hu. Visual attention network. *arXiv preprint arXiv:2202.09741*, 2022.

[14] K. He, X. Chen, S. Xie, Y. Li, P. Dollár, and R. Girshick. Masked autoencoders are scalable vision learners. In *Proceedings of the IEEE/CVF Conference on Computer Vision and Pattern Recognition*, 2022.

[15] S. Hochreiter and J. Schmidhuber. Long short-term memory. *Neural computation*, 9(8):1735–1780, 1997.

[16] J.-T. Hsieh, B. Liu, D.-A. Huang, L. F. Fei-Fei, and J. C. Niebles. Learning to decompose and disentangle representations for video prediction. *Advances in Neural Information Processing Systems*, 31, 2018.

[17] X. Hu, Z. Huang, A. Huang, J. Xu, and S. Zhou. A dynamic multi-scale voxel flow network for video prediction. In *Proceedings of the IEEE/CVF Conference on Computer Vision and Pattern Recognition (CVPR)*, 2023.

[18] C. Ionescu, D. Papava, V. Olaru, and C. Sminchisescu. Human3.6m: Large scale datasets and predictive methods for 3d human sensing in natural environments. *IEEE transactions on pattern analysis and machine intelligence*, 36(7):1325–1339, 2013.

[19] S. Jenni, G. Meishvili, and P. Favaro. Video representation learning by recognizing temporal transformations. In *European Conference on Computer Vision*, pages 425–442. Springer, 2020.

[20] A. Krizhevsky, G. Hinton, et al. Learning multiple layers of features from tiny images. 2009.

[21] K. Li, Y. Wang, J. Zhang, P. Gao, G. Song, Y. Liu, H. Li, and Y. Qiao. Uniformer: Unifying convolution and self-attention for visual recognition. *arXiv preprint arXiv:2201.09450*, 2022.

https://doi.org/10.52202/075280-3060

[22] S. Li, Z. Wang, Z. Liu, C. Tan, H. Lin, D. Wu, Z. Chen, J. Zheng, and S. Z. Li. Efficient multi-order gated aggregation network. *arXiv preprint arXiv:2211.03295*, 2022.

[23] S. Li, Z. Wang, Z. Liu, D. Wu, C. Tan, and S. Z. Li. Openmixup: Open mixup toolbox and benchmark for visual representation learning. *ArXiv*, abs/2209.04851, 2022.

[24] S. Li, D. Wu, F. Wu, Z. Zang, K. Wang, L. Shang, B. Sun, H. Li, and Stan.Z.Li. Architecture-agnostic masked image modeling - from vit back to cnn. In *International Conference on Machine Learning (ICML)*, 2023.

[25] X. Liu, J. Yin, J. Liu, P. Ding, J. Liu, and H. Liu. Trajectorycnn: a new spatio-temporal feature learning network for human motion prediction. *IEEE Transactions on Circuits and Systems for Video Technology*, 31(6):2133–2146, 2020.

[26] Z. Liu, Y. Lin, Y. Cao, H. Hu, Y. Wei, Z. Zhang, S. Lin, and B. Guo. Swin transformer: Hierarchical vision transformer using shifted windows. In *Proceedings of the IEEE/CVF International Conference on Computer Vision*, pages 10012–10022, 2021.

[27] Z. Liu, H. Mao, C.-Y. Wu, C. Feichtenhofer, T. Darrell, and S. Xie. A convnet for the 2020s. *arXiv preprint arXiv:2201.03545*, 2022.

[28] Z. Liu, R. A. Yeh, X. Tang, Y. Liu, and A. Agarwala. Video frame synthesis using deep voxel flow. In *Proceedings of the IEEE International Conference on Computer Vision*, pages 4463–4471, 2017.

[29] W. Lotter, G. Kreiman, and D. Cox. Deep predictive coding networks for video prediction and unsupervised learning. In *International Conference on Learning Representations*, 2017.

[30] M. Oliu, J. Selva, and S. Escalera. Folded recurrent neural networks for future video prediction. In *Proceedings of the European Conference on Computer Vision (ECCV)*, pages 716–731, 2018.

[31] S. Oprea, P. Martinez-Gonzalez, A. Garcia-Garcia, J. A. Castro-Vargas, S. Orts-Escolano, J. Garcia-Rodriguez, and A. Argyros. A review on deep learning techniques for video prediction. *IEEE Transactions on Pattern Analysis and Machine Intelligence*, 2020.

[32] R. Qian, T. Meng, B. Gong, M.-H. Yang, H. Wang, S. Belongie, and Y. Cui. Spatiotemporal contrastive video representation learning. In *Proceedings of the IEEE/CVF Conference on Computer Vision and Pattern Recognition*, pages 6964–6974, 2021.

[33] Y. Rao, W. Zhao, Y. Tang, J. Zhou, S. N. Lim, and J. Lu. Hornet: Efficient high-order spatial interactions with recursive gated convolutions. *Advances in Neural Information Processing Systems*, 35:10353–10366, 2022.

[34] S. Rasp, P. D. Dueben, S. Scher, J. A. Weyn, S. Mouatadid, and N. Thuerey. Weatherbench: a benchmark data set for data-driven weather forecasting. *Journal of Advances in Modeling Earth Systems*, 12(11):e2020MS002203, 2020.

[35] M. Reichstein, G. Camps-Valls, B. Stevens, M. Jung, J. Denzler, N. Carvalhais, et al. Deep learning and process understanding for data-driven earth system science. *Nature*, 566(7743):195–204, 2019.

[36] C. Schuldt, I. Laptev, and B. Caputo. Recognizing human actions: a local svm approach. In *Proceedings of the 17th International Conference on Pattern Recognition, 2004. ICPR 2004.*, volume 3, pages 32–36. IEEE, 2004.

[37] M. seok Seo, H. Lee, D.-Y. Kim, and J. Seo. Implicit stacked autoregressive model for video prediction. *ArXiv*, abs/2303.07849, 2023.

[38] X. Shi, Z. Chen, H. Wang, D.-Y. Yeung, W.-K. Wong, and W.-c. Woo. Convolutional lstm network: A machine learning approach for precipitation nowcasting. *Advances in Neural Information Processing Systems*, 28, 2015.

[39] N. Srivastava, E. Mansimov, and R. Salakhudinov. Unsupervised learning of video representations using lstms. In *International conference on machine learning*, pages 843–852. PMLR, 2015.

[40] C. Tan, Z. Gao, S. Li, and S. Z. Li. Simvp: Towards simple yet powerful spatiotemporal predictive learning. *arXiv preprint arXiv:2211.12509*, 2022.

[41] C. Tan, Z. Gao, L. Wu, Y. Xu, J. Xia, S. Li, and S. Z. Li. Temporal attention unit: Towards efficient spatiotemporal predictive learning. In *Proceedings of the IEEE/CVF Conference on Computer Vision and Pattern Recognition*, 2023.

[42] I. O. Tolstikhin, N. Houlsby, A. Kolesnikov, L. Beyer, X. Zhai, T. Unterthiner, J. Yung, A. Steiner, D. Keysers, J. Uszkoreit, et al. Mlp-mixer: An all-mlp architecture for vision. *Advances in neural information processing systems*, 34:24261–24272, 2021.

[43] A. Trockman and J. Z. Kolter. Patches are all you need? *arXiv preprint arXiv:2201.09792*, 2022.

[44] R. Villegas, D. Erhan, H. Lee, et al. Hierarchical long-term video prediction without supervision. In *International Conference on Machine Learning*, pages 6038–6046. PMLR, 2018.

[45] P. Wang, W. Li, P. Ogunbona, J. Wan, and S. Escalera. Rgb-d-based human motion recognition with deep learning: A survey. *Computer Vision and Image Understanding*, 171:118–139, 2018.

[46] Y. Wang, H. Chen, Y. Fan, W. Sun, R. Tao, W. Hou, R. Wang, L. Yang, Z. Zhou, L.-Z. Guo, et al. Usb: A unified semi-supervised learning benchmark for classification. *Advances in Neural Information Processing Systems*, 35:3938–3961, 2022.

[47] Y. Wang, Z. Gao, M. Long, J. Wang, and S. Y. Philip. Predrnn++: Towards a resolution of the deep-in-time dilemma in spatiotemporal predictive learning. In *International Conference on Machine Learning*, pages 5123–5132. PMLR, 2018.

[48] Y. Wang, L. Jiang, M.-H. Yang, L.-J. Li, M. Long, and L. Fei-Fei. Eidetic 3d lstm: A model for video prediction and beyond. In *International conference on learning representations*, 2018.

[49] Y. Wang, M. Long, J. Wang, Z. Gao, and P. S. Yu. Predrnn: Recurrent neural networks for predictive learning using spatiotemporal lstms. *Advances in Neural Information Processing Systems*, 30, 2017.

[50] Y. Wang, H. Wu, J. Zhang, Z. Gao, J. Wang, P. S. Yu, and M. Long. Predrnn: A recurrent neural network for spatiotemporal predictive learning. *arXiv preprint arXiv:2103.09504*, 2021.

[51] Y. Wang, J. Zhang, H. Zhu, M. Long, J. Wang, and P. S. Yu. Memory in memory: A predictive neural network for learning higher-order non-stationarity from spatiotemporal dynamics. In *Proceedings of the IEEE/CVF Conference on Computer Vision and Pattern Recognition*, pages 9154–9162, 2019.

[52] Z. Wang, A. C. Bovik, H. R. Sheikh, and E. P. Simoncelli. Image quality assessment: from error visibility to structural similarity. *IEEE transactions on image processing*, 13(4):600–612, 2004.

[53] H. Wu, W. Xion, F. Xu, X. Luo, C. Chen, X. Hua, and H. Wang. Pastnet: Introducing physical inductive biases for spatio-temporal video prediction. *ArXiv*, abs/2305.11421, 2023.

[54] L. Wu, H. Lin, Z. Gao, C. Tan, and S. Z. Li. Graphmixup: Improving class-imbalanced node classification on graphs by self-supervised context prediction. *European Conference on Machine Learning*, 2022.

[55] L. Wu, H. Lin, Y. Huang, and S. Z. Li. Knowledge distillation improves graph structure augmentation for graph neural networks. *Advances in Neural Information Processing Systems*, 2022.

[56] L. Wu, H. Lin, C. Tan, Z. Gao, and S. Z. Li. Self-supervised learning on graphs: Contrastive, generative, or predictive. *IEEE Transactions on Knowledge and Data Engineering*, 2021.

[57] Z. Xu, Y. Wang, M. Long, J. Wang, and M. KLiss. Predcnn: Predictive learning with cascade convolutions. In *IJCAI*, pages 2940–2947, 2018.

[58] W. Yu, Y. Lu, S. Easterbrook, and S. Fidler. Efficient and information-preserving future frame prediction and beyond. In *International Conference on Learning Representations*, 2019.

[59] W. Yu, M. Luo, P. Zhou, C. Si, Y. Zhou, X. Wang, J. Feng, and S. Yan. Metaformer is actually what you need for vision. In *Proceedings of the IEEE/CVF conference on computer vision and pattern recognition*, pages 10819–10829, 2022.

[60] J. Zhang, Y. Zheng, and D. Qi. Deep spatio-temporal residual networks for citywide crowd flows prediction. In *Thirty-first AAAI conference on artificial intelligence*, 2017.

[61] L. Zhang, G. Zhu, P. Shen, J. Song, S. Afaq Shah, and M. Bennamoun. Learning spatiotemporal features using 3dcnn and convolutional lstm for gesture recognition. In *Proceedings of the IEEE International Conference on Computer Vision Workshops*, pages 3120–3128, 2017.

[62] R. Zhang, P. Isola, A. A. Efros, E. Shechtman, and O. Wang. The unreasonable effectiveness of deep features as a perceptual metric. In *Proceedings of the IEEE conference on computer vision and pattern recognition*, pages 586–595, 2018.

https://doi.org/10.52202/075280-3060